Macromolecules
ARTICLE

Macromolecules **2010**, *43*, 4733–4743 **4733**
DOI: 10.1021/ma902866x

NEXAFS Depth Profiling of Surface Segregation in Block Copolymer Thin Films

Sitaraman Krishnan,*,† Marvin Y. Paik,‡ Christopher K. Ober,‡ Elisa Martinelli,§ Giancarlo Galli,§ Karen E. Sohn,⊥ Edward J. Kramer,∥ and Daniel A. Fischer○

†*Clarkson University, Department of Chemical and Biomolecular Engineering, Potsdam, New York 13699,* ‡*Department of Materials Science and Engineering, Cornell University, Ithaca, New York 14850,* §*Dipartimento di Chimica e Chimica Industriale and UdR Pisa INSTM, Università di Pisa, 56126 Pisa, Italy,* ⊥*Department of Materials, University of California, Santa Barbara, California 93106,* ∥*Departments of Materials and Chemical Engineering, University of California, Santa Barbara, California 93106, and* ○*National Institute of Standards and Technology, Gaithersburg, Maryland 20899*

Received January 9, 2010; Revised Manuscript Received March 30, 2010

ABSTRACT: NEXAFS spectroscopy was used to probe the surface composition and under-water surface reconstruction of thin films of comb-like diblock copolymers with cylindrical and spherical microphases. The polymers consisted of a polystyrene block, and a second block prepared from a styrenic monomer grafted with fluoroalkyl-tagged poly(ethylene glycol) side chains. Compositional depth profiling of the microphase separated block copolymer films, in the top 1−3 nm of the film, was performed to understand the role of block copolymer microstructure and self-assembly on surface composition. Using experimentally determined concentration profiles, the surface concentration of phenyl ring carbon atoms was quantified and compared with those of homopolymer and random copolymer controls. The carbon atoms from the relatively high surface energy phenyl groups were depleted or excluded from the surface, in favor of the low surface-energy fluoroalkyl groups. While it is expected that block copolymer surfaces will be completely covered by a wetting lamellar layer of the lower surface energy block, a significant amount of the higher surface energy polystyrene block was found to be present in the surface region of the cylinder-forming block copolymer. Evidently, the spontaneous formation of the cylindrical polystyrene microdomains in the near-surface region compensated for the lowering of the free energy that could have been achieved by completely covering the surfaces with a lamellar layer of the lower surface energy fluorinated block. All surfaces underwent molecular reconstruction after immersion in water. The experimental concentration depth profiles indicated an increased surface depletion of phenyl ring carbon atoms in the water-immersed thin films, due to the tendency of hydrophilic PEG side groups to be present at the polymer−water interface. Such a detailed characterization of the outermost layers of the block copolymer surfaces was possible because of the exceptional depth resolution of the NEXAFS depth profiling technique.

1. Introduction

There is currently a considerable interest in using patterned surfaces of amphiphilic block copolymers[1,2] and other nanostructured polymers[3] for controlling interactions of proteins and cells with surfaces. The fact that interaction of amphiphilic biomolecules such as proteins,[4] and even cells and microorganisms, are sensitive to surface chemical heterogeneities[5] has triggered interest in developing functional block copolymers as antibiofouling coatings. Block copolymer self-assembly is a viable approach to create large-area nanopatterned coatings, with tunable pattern size and shape.[6−8] Because biological interactions of such patterned coatings usually occur in an aqueous environment, it is important to study the influence of water on the surface composition of the block copolymer coatings. Polymer surfaces can undergo significant reconstruction when immersed in water,[9−14] such that the composition at the water−polymer interface could be quite different from the composition at the air−polymer interface. Few publications have investigated the effect of water on chemical structures of block copolymer films using surface sensitive spectroscopic techniques.[2,3,7,15,16]

*To whom correspondence should be addressed. E-mail: skrishna@clarkson.edu.

We are interested in the near-surface molecular organization, and reorganization upon immersion in water, of comb-like block copolymers with PEGylated fluoroalkyl side chains (cf. Figure 1). The surface active side chains of these polymers consist of a hydrophilic, poly(ethylene glycol) (PEG) segment that is directly linked to a hydrophobic perfluoroalkyl segment. Block copolymers, with polystyrene, show sufficient chemical incompatibility between the two blocks to result in spontaneous formation of block copolymer microdomains. In air, the low surface energy perfluoroalkyl segment is expected to cause surface segregation of moieties that are attached to it. Under water, the hydrophilic ethylene glycol segments will result in accumulation of these side chains at the water−polymer interface. Block copolymers with these PEGylated fluoroalkyl side groups have shown excellent resistance to adhesion by marine organisms and the adsorption of biomolecules such as proteins.[7,8,17] Fluoroalkyl-tagged poly(ethylene glycol) moieties, similar to the side chains of the polymers of the present study, have also been used for drug delivery[18] and oil−water separation.[19]

When one of the blocks in a block copolymer contains fluoroalkyl groups in the side chains, preferential accumulation of the lower surface energy block at the surface may alter the block copolymer morphology in the near surface region to be

Published on Web 04/22/2010

significantly different from that in the bulk. This is often the case in block copolymers with semifluorinated liquid crystalline side chains, as reviewed in ref 20. A highly surface sensitive chemical spectroscopic technique, with subnanometer depth resolution, is required to verify whether the microphase separation seen in the bulk of the polymer thin film is also displayed at the surface of the coating. Such a study is relevant in the context of attempts to create nanopatterned chemically heterogeneous surfaces using block copolymer self-assembly.

A variety of depth profiling techniques have been used in the past to study the structure of polymers near surfaces and interfaces,[21,22] but the depth resolution of these techniques is generally not sufficient to probe molecular composition in the top 1−3 nm of a surface. Techniques such as forward recoil spectrometry (FRES), nuclear reaction analysis (NRA), and dynamic secondary ion mass spectrometry (SIMS) have the advantage of a direct, model-independent determination of depth profiles, and generally have depth resolutions ranging from 10 to 800 nm.[23] Using grazing incidence geometry, an improvement in depth resolution, down to about 3 nm has been achieved in NRA.[24] Neutron reflectivity (NR) and X-ray reflectivity (XR) techniques, which have at least 1 order of magnitude better depth resolution (0.5−4 nm), are well-established techniques for determining film thickness, interfacial width, and interfacial roughness values with subnanometer precision. Moreover, in a relatively new X-ray approach called resonant soft X-ray reflectivity (RSoXR), molecular-structure specific variations in the complex index of refraction has been used to augment conventional XR with molecular spectroscopy capability.[25] X-ray photoelectron spectroscopy (XPS) has been widely used for depth profiling of polymer thin films.[26−29] Using an electron emission angle, φ, of 85° measured from surface normal, sampling depths as low as 0.5−0.75 nm have been achieved,[30] although it may be necessary to incorporate elastic scattering effects in reconstruction of composition-depth profile from angle-resolved XPS data acquired at such large emission angles.[31]

NEXAFS analysis is a powerful spectroscopic technique for composition depth profiling, well-suited for probing low atomic-number atoms such as C, N, O, and F that are the main constituents of several organic polymers.[32] Chemical modification of the polymer (for example, deuteration) is not necessary for depth profiling, and as will be evident from this report, C K-edge NEXAFS has exceptional sensitivity to subnanometer depth variations in atomic concentrations. Although the sampling-depth in C K-edge NEXAFS analysis is limited to below 5 nm, and the technique cannot be used to study interfaces buried below this depth, molecular composition of the top few nanometers of a surface can be accurately characterized. In principle, a model-independent determination of compositional depth profile is possible using NEXAFS depth-profiling. In the present study, however, a model for composition profile was selected *a priori*, and the experimental NEXAFS data were used to determine the parameters of this model.

There are only a few studies that have used NEXAFS to determine near-surface composition profiles in polymer thin films. In the past, we have used NEXAFS to characterize composition depth profile in thermally annealed amphiphilic block copolymer thin films.[7,38] Theato et al. have studied surface reorganization of polymer films prepared from diblock copolymers comprised of a polystyrene block and a second hydrophilic polystyrene block with acetoxy-terminated diethylene glycol side chains.[16] Using NEXAFS spectroscopy, it was demonstrated that the outermost surface layer exhibited an exchange between hydrophobic and hydrophilic segments as the surfaces were equilibrated in vacuum and water, respectively.[33] While interfacial segregation was clearly evident from their NEXAFS analysis, composition depth profiles were not the focus of investigation.

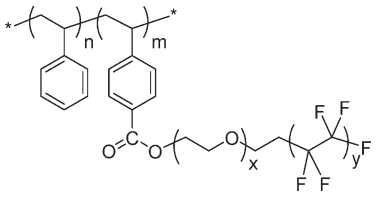

Figure 1. Copolymers with amphiphilic, PEGylated fluoroalkyl side chains: $\langle x \rangle \sim 5$ and $\langle y \rangle \sim 4$.

Table 1. Microstructure Characterization of Polymers Used in the Present Study

					d-spacing (nm)	
polymer	type	m^a	v^b	microdomains	AFM	GISAXS
H	homopolymer	1.00	1.00			
R	random copolymer	0.66	0.91			
S	block copolymer	0.28	0.67	PS spheres	23.0	22.0
C	block copolymer	0.25	0.63	PS lying cylinders	19.8	20.3

[a] m is the mole fraction of the monomer with PEGylated fluoroalkyl side chains. [b] v is the volume fraction of the monomer with PEGylated fluoroalkyl side chains.

In the present paper, we discuss the effect of surface segregation on the near-surface composition profile of amphiphilic block copolymers, and the role of water in restructuring the surface. Quantitative depth profiles were obtained for surfaces immersed in water (prior to NEXAFS analysis) and were compared with near-surface structure of surfaces annealed *in vacuo*, to understand the surface-reconstruction phenomenon.

2. Materials and Methods

Four different polymers were investigated. The structure of the polymers is shown in Figure 1. The PEGylated fluoroalkyl side chains were polydisperse, with average number of ethylene glycol units, $\langle x \rangle$, equal to 5, and the average number of perfluoroethylene groups, $\langle y \rangle$, equal to 4. Table 1 gives structural details of these polymers determined using ^{1}H NMR spectroscopy, size exclusion chromatography, grazing incidence small-angle X-ray scattering (GISAXS), and atomic force microscopy (AFM). The polymers are denoted by **H**, **R**, **S**, and **C**. Polymer **H** is a homopolymer of the styrenic monomer with PEGylated fluoroalkyl side chains. Polymer **R** is a random copolymer of styrene and the PEGylated/fluorinated monomer. Polymer **S** is a block copolymer with spherical microdomains of polystyrene dispersed in a matrix of the PEGylated/fluorinated block. Polymer **C** is a block copolymer with a cylindrical polystyrene microdomains. The mole fraction of the amphiphilic monomer in the copolymer, denoted by m in Table 1, was determined by ^{1}H NMR spectroscopy. The block copolymers were synthesized by atom transfer radical polymerization (ATRP). Homopolymer **H** and random copolymer **R** were synthesized by conventional free radical polymerization using 2,2′-azobis(isobutyronitrile) initiator. Details on the synthesis of the PEGylated/fluororinated monomer and the block copolymers, spectroscopic (IR and NMR) and thermal (DSC) characterization of the polymers, along with preliminary surface characterization using contact angle measurements and X-ray absorption spectroscopy have been reported previously.[15] The block copolymer microstructures and domain sizes were determined by AFM and GISAXS, as also reported previously.[15]

The PEGylated/fluorinated monomer was the majority component in all the three copolymers, which is evident from the volume fractions, v, shown in Table 1. Molecular weights and polydispersity indices (PDI) were determined by size exclusion

chromatography (SEC, Jasco PU-1580 liquid chromatograph equipped with a Jasco 830-RI refractive index detector and a Perkin-Elmer LC75 UV detector) of dilute polymer solutions in chloroform, using polystyrene standards for hydrodynamic volume versus molecular weight calibration. The number-average molecular weights, $\bar{M}_n$, of the PS block in block copolymers **S** and **C** were 5300 g/mol ($\bar{M}_w/\bar{M}_n = 1.37$). The total number-average molecular weight, determined by GPC, was 22 800 g/mol for polymer **S** and 16 000 g/mol for polymer **C**. The ratios of the weight-average and number-average molecular weights were 1.77 for **S** and 1.51 for **C**. The ATRP controlled radical polymerization resulted in polymers with narrower molecular weight distributions than conventional free radical polymerization, as evident from the relative widths of the SEC chromatograms (cf. Supporing Information). The volume fraction of the amphiphilic monomer in the copolymer thin film was calculated using the molar volume of the amphiphilic monomer, estimated using group contribution values for molar volume[34] (cf. Table 1). The two block copolymers used in the present study evidently had compositions at the border between spherical and cylindrical regions of the block copolymer phase diagram. The glass transition temperature of the PEGylated/fluorinated homopolymer was determined to be −35 °C using differential scanning calorimetry (Mettler DSC-30). The relatively low molecular weight PS blocks in the block copolymers showed glass transition near 85 °C. The microdomain *d*-spacings determined using GISAXS were about 22 and 20 nm for block copolymers **S** and **C**, respectively.

The polymers were dissolved in chloroform to obtain 3% (w/v) solutions. The solutions were filtered using a 450 nm syringe filter and spin-coated on silicon wafers. A Cee model 100CB spin coater was used at a rotational speed of 2000 rpm for 30 s (acceleration of 1000 rpm/s). The films were dried in a vacuum oven at 60 °C and further annealed *in vacuo* at 120 °C for 12 h. They were then slowly cooled to room temperature. These surfaces will be referred to as "dry" surfaces. The thicknesses of the films were measured using the Woollam variable angle spectroscopic ellipsometer. The spectral data were collected over a wavelength range from 300 to 1000 nm at an angle of incidence of 70°. The data from the polymer thin film layer was evaluated using a Cauchy model. The dry thicknesses of **H**, **R**, **S**, and **C** films were all found to be between 400 and 550 nm thick, significantly larger than the sampling depth of NEXAFS, and the block copolymer domain sizes. A Veeco Digital Instruments Dimension 3100 scanning probe microscope was used in the tapping mode for AFM measurements.

Dynamic water contact angle values were determined using the sessile drop method. Advancing and receding water contact angles were measured at room temperature using a Ramé-Hart model 100−00 contact angle goniometer. A droplet on the surface was expanded and contracted by the addition and withdrawal, respectively, of water using a microsyringe and needle assembly. The advancing contact angle, θ_a, was measured at the leading edge of the expanding droplet, and the receding contact angle, θ_r, was measured at the trailing edge of the contracting droplet.

X-ray photoelectron spectroscopy (XPS) of surfaces were performed using a Surface Science Instruments SSX-100 with a monochromatic Al Kα X-ray source at 1486.6 eV at an operating pressure of less than 2×10^{-9} Torr. Photoelectrons were collected at an angle of 55° from the surface normal and analyzed using a hemispherical analyzer with pass energy of 150 eV for survey scans and 50 eV for high resolution scans. The X-ray incidence angle, relative to the surface normal, was 71°. Charge compensation was carried out using low-energy electrons from an electron flood gun. The spectra were analyzed using CasaXPS v. 2.3.12 software.

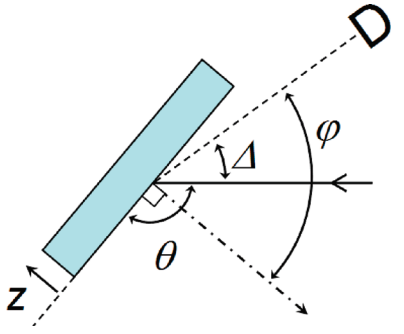

Figure 2. Schematic of the experimental geometry. θ is the angle of X-ray incidence. **D** is the channeltron electron detector, which is at a fixed angle Δ with respect to the X-ray beam. Emission angle φ is the angle between the surface normal and the path traversed by the electrons to reach the detector. The sample is rotated about an axis normal to the plane of the figure to vary θ (and φ).

To study under-water surface reconstruction, the thermally annealed surfaces were immersed in distilled water for 3 days at room temperature and subsequently for 12 h at 70 °C. The surfaces were kept immersed in water at room temperature, and were removed from water and dried at room temperature just before loading into the NEXAFS analysis chamber. These surfaces, which had been immersed in water prior to X-ray analysis, will be referred to as "wet" surfaces. A comparison of the NEXAFS spectra of the wet surfaces, acquired at different times in the NEXAFS chamber, indicated that the surfaces underwent negligible reconstruction *in vacuo* at room temperature—over the time scale of the NEXAFS experiments (cf. Supporting Information).

NEXAFS depth profiling experiments were carried out on the U7A NIST/Dow materials characterization end-station at the National Synchrotron Light Source at Brookhaven National Laboratory. The synchrotron X-ray beam was elliptically polarized (polarization factor, $P = 0.85$), with the electric field vector predominantly in the plane of the storage ring. The photon flux was about 10^{11} photons/s at a typical storage ring current of 500 mA. A spherical grating monochromator was used to obtain monochromatic soft X-rays at an energy resolution of 0.1 eV. Spectra were acquired at 0.2 eV steps. C K-shell NEXAFS spectra were acquired for photon energy in the range 270−320 eV. The NEXAFS chamber consisted of a sample holder that was positioned on a computer-controlled goniometer. The sample holder could be rotated about an axis normal to the plane of the storage ring to vary the X-ray incidence angle, θ (Figure 2). NEXAFS spectra were obtained at X-ray incidence angles varying from 20° to 130°.[35] Each measurement was taken on a fresh spot to minimize possible beam damage effects. Electrons emitted from the surface were collected using a channeltron electron multiplier with an adjustable entrance grid bias (EGB). The data reported were acquired using a grid bias of −150 V. The negative grid potential prevents electrons with kinetic energy less than 150 eV from entering the detector. The channeltron partial electron yield (PEY) detector was positioned at an angle, Δ, of 36° with respect to the incoming X-ray beam, and in the equatorial plane of the sample chamber. Thus, the emission angle, φ, is given by $\varphi = \theta + \Delta - 90°$ (Figure 2).

To eliminate the effect of incidence beam intensity variations and monochromator absorption features, the PEY signals were normalized by the incidence beam intensity obtained from the photo yield of a clean gold grid. A linear pre-edge baseline was subtracted from the normalized spectra, and the edge jump was arbitrarily set to unity far above the C K-edge, a procedure that enabled comparison of different NEXAFS spectra for the same number of carbon atoms.[36] Energy calibration was performed

using a highly oriented pyrolytic graphite (HOPG) reference sample. The HOPG C 1s → π^* transition was assigned an energy of 285.5 eV according to the literature value.[37] The simultaneous measurement of a graphite-coated gold grid allowed the calibration of the photon energy with respect to the HOPG sample. The error in the energy calibration is expected to be within ±0.5 eV. Charge compensation was carried out by directing low-energy electrons from an electron gun onto the sample surface.

Depth profiling using NEXAFS is also possible by using a fixed angle of X-ray incidence, but varying the entrance grid bias of the channeltron electron detector.[38−40] In the present study, however, we varied the X-ray incidence angle at a constant value of the entrance grid bias.

3. Model Description

As shown in eq 1, the postedge normalized Auger electron intensity, I_a, depends on the flux, I_0 (photons s^{-1} cm^{-2}), of the incidence X-ray photons; the area, A_0 (cm^2), of the sample exposed to the X-ray beam; the X-ray absorption cross section, $\sigma_{x,i}$, corresponding to electronic transition i; the Auger electron yield, ω_a, of the core excitation process; the concentration, ρ_i (atoms/cm^3) of carbon atoms involved in a chemical bond of type i; the escape depth of electrons, λ_i (nm); and the angle of emission with respect to the surface normal, φ, at which the electrons are detected.[7]

$$I_a = \frac{\int_0^\infty I_0 A_0 \sigma_{x,i} \rho_i(z) \omega_a \exp\left\{-\frac{z}{\lambda_i \cos\varphi}\right\} dz}{\sum_i \int_0^\infty I_0 A_0 \sigma_{x,i} \rho_i(z) \omega_a \exp\left\{-\frac{z}{\lambda_i \cos\varphi}\right\} dz} \quad (1)$$

The summation in the denominator of eq 1 is of Auger emissions from all the carbon atoms in the sample that have different bonding environments, measured typically at around 320 eV for the C 1s NEXAFS spectra—an energy that corresponds to electronic transition to the continuum state. It should be noted that only those electrons that have kinetic energy higher than the retarding potential applied at the electron detector are measured.

The kinetic energy of the Auger electrons emitted, when core holes at different carbon atoms are filled, is nearly identical. Consequently, the electron escape depths, λ_i, can be replaced by a common value, λ. Similarly, the X-ray absorption cross section for electronic transitions to a continuum ($\sigma_{x,i}$ in the denominator of eq 1) is insensitive to the nature of chemical bonding, and is the same for all carbon atoms. Hence, eq 1 can be simplified to:

$$I_a = \frac{\int_0^\infty \sigma_{x,i} \rho_i(z) \exp\left\{-\frac{z}{\lambda \cos\varphi}\right\} dz}{\sigma_x|_{320\ eV} \int_0^\infty \{\sum_i \rho_i(z)\} \exp\left\{-\frac{z}{\lambda \cos\varphi}\right\} dz} \quad (2)$$

The absorption cross section for transition to a σ^* or a π^* final state, however, depends not only on chemical bonding but also on the orientation of bonds with respect to the electric field of the polarized X-ray beam such that

$$\sigma_{x,i} \propto \cos^2 \delta \quad (3)$$

where δ is the angle between the direction of the electric field vector and the direction of the final state molecular orbital.[41] In the case of phenyl rings, the direction of the π^* orbital is perpendicular to the plane of the phenyl ring. When the bond orientation exhibits azimuthal symmetry about the surface normal, as is expected to be the case here, eq 3 can be expressed in terms of the X-ray incidence angle, θ, and the orbital tilt angle, α, as follows:

$$\sigma_{x,i} \propto P \cos^2\theta \left(1 - \frac{3}{2}\sin^2\alpha\right) + \frac{1}{2}\sin^2\alpha \quad (4)$$

where P is the degree of polarization of the X-ray beam, equal to about 0.85. Notational simplification can be achieved by using the definition of bond orientational order parameter, S

$$S = 1 - \frac{3}{2}\langle \sin^2\alpha \rangle \quad (5)$$

where $\langle \sin^2\alpha \rangle$ is the average of $\sin^2\alpha$ over all the bonds.

Thus,

$$\sigma_{x,i} \propto PS \cos^2\theta + \frac{1-S}{3} \quad (6)$$

Equation 2 can be further simplified by assuming that the atomic density of carbon atoms in the polymer thin film is independent of depth,[42,43] to obtain:

$$I_a = \frac{\int_0^\infty \sigma_{x,i} f_i(z) \exp\left\{-\frac{z}{\lambda \cos\varphi}\right\} dz}{\sigma_x|_{320\ eV} \lambda \cos\varphi} \quad (7)$$

where

$$f_i(z) = \rho_i(z) / \sum_i \rho_i(z)$$

is the ratio of the number density of carbon atoms that belong to a chemical bond of type i, at depth z, to the total number density of carbon atoms, at depth z. Combining eqs 6 and 7, we get

$$I_a = \frac{A}{3\lambda \cos\varphi} \int_0^\infty f_i(z) \exp\left\{-\frac{z}{\lambda \cos\varphi}\right\} dz + \frac{A}{\lambda \cos\varphi}\left(P\cos^2\theta - \frac{1}{3}\right) \int_0^\infty S(z) f_i(z) \exp\left\{-\frac{z}{\lambda \cos\varphi}\right\} dz \quad (8)$$

where A is a proportionality constant.

Equation 8 relates the variation in the normalized intensity of a NEXAFS resonance to physical characteristics of the film, namely, composition, f_i, and bond orientation, S, and the geometrical features of the experimental setup, namely, angle of X-ray incidence, θ, and angle of electron detection, φ. By measuring resonance intensities over a series of X-ray incidence and electron detection angles, it is possible to extract information on compositional depth profile and molecular orientation in the thin film.

The order parameter, S, can be constant throughout the thickness of the film or can vary with depth. For constant S, eq 8 can be rewritten as

$$I_a = \frac{A}{\lambda \cos\varphi}\left\{\frac{1}{3} + \left(P\cos^2\theta - \frac{1}{3}\right)S\right\} \int_0^\infty f_i(z) \exp\left\{-\frac{z}{\lambda \cos\varphi}\right\} dz \quad (9)$$

The order parameter will be equal to 0 when the bonds are not ordered. Here, the second integral on the right-hand side of eq 8 drops out, resulting in the equation that we derived previously.[7]

4. Results and Discussion

4.1. Homopolymer Thin Films. Figure 3 shows the XPS survey scan for the homopolymer surface. The experimentally determined atomic concentrations are in good agreement with

the values expected from the known chemical structure of the homopolymer: C 55.1% (54.7% expected); O 13.2% (13.3% expected); and F 31.6% (32.1% expected). The high resolution C 1s XPS spectrum is shown in the Supporting Information.

Figure 4 shows the NEXAFS spectrum of a dry film of homopolymer **H**, obtained using an X-ray incidence angle of 50°. Curve fitting of the C 1s spectrum was performed using a series of Voigt, Gaussian and asymmetric Gaussian line shapes, as discussed by Stöhr.[36] A square step function, convoluted with a Gaussian function and an exponential decay function, was used to model the continuum step. The curve fits are shown in Figure 4. The peak near 285.2 eV corresponds to the C 1s → $\pi^*_{C=C}$ resonance,[44−46] whereas that near 293 eV corresponds to the C 1s → σ^*_{C-F} resonance.

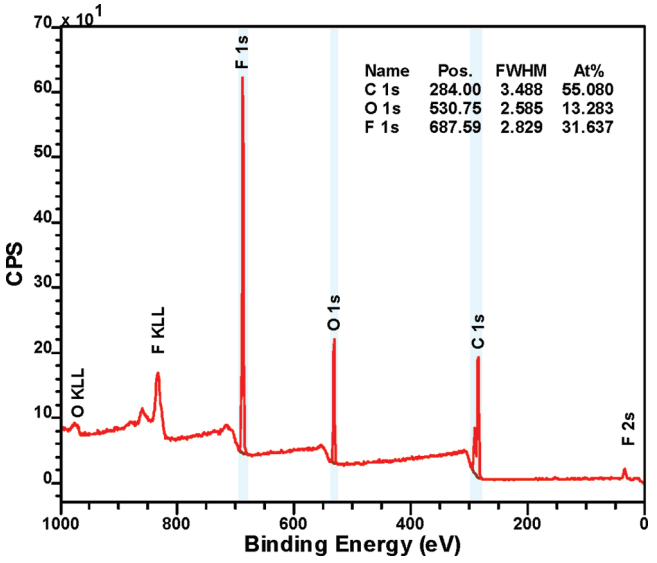

Figure 3. XPS spectrum of a surface of a dry film of homopolymer **H** obtained at an emission angle of 55° relative to surface normal.

4.2. Copolymer Thin Films. Figure 5 shows the postedge normalized C 1s NEXAFS spectra of "dry" surfaces of copolymers **C**, **S**, and **R**, acquired at an X-ray incidence angle of 50°.

The $\pi^*_{C=C}$ peak intensity was higher for "dry" block copolymer **C** than "dry" homopolymer **H** (cf. Figure 4). The normalized PEY of C 1s → $\pi^*_{C=C}$ resonance at 50° X-ray incidence was about 2.66 for the "dry" block copolymer **C** and 1.86 for "dry" homopolymer **H**. Thin films of block copolymer **C** contained cylindrical PS microdomains that were oriented parallel to the substrate (cf. tapping mode AFM-phase image shown in Figure 6). Clearly, the higher intensity of the $\pi^*_{C=C}$ resonance is because of the styrene units from the polystyrene block that are present either at the surface ($z/\lambda = 0$) or very close to the surface (within a depth of about $3\lambda \approx 6$ nm that is probed by NEXAFS).

Surfaces of diblock copolymers in which the block with lower surface energy is the majority component (as in the case of the block copolymers of the present study) are expected to be completely covered, at equilibrium, by a thin brush layer of the lower surface energy block, irrespective of the block copolymer microstructure in the bulk.[47] In a recent study using tapping mode atomic force microscopy, X-ray photoelectron spectroscopy, neutron reflectometry, and surface wettability measurements, Neto et al. found that surfaces of thin films of polystyrene-*block*-poly(ethylene oxide) (PS-*b*-PEO) diblock copolymer, with lamellar morphology, were completely covered by the lower surface-energy

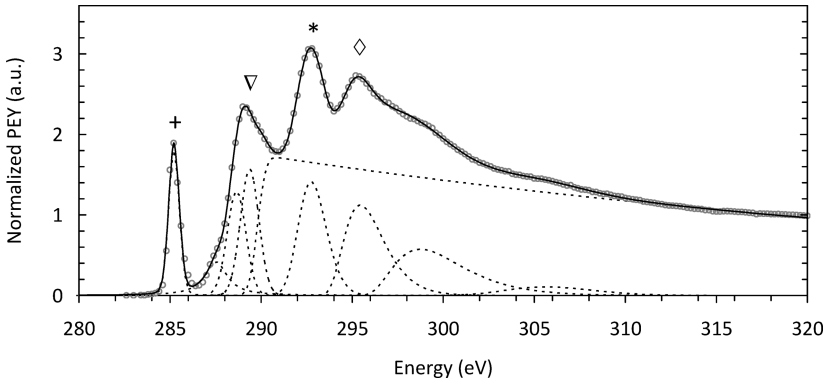

Figure 4. Carbon K-edge NEXAFS spectrum of homopolymer **H** and the fitted curves. The spectrum was acquired at an X-ray incidence angle of 50° and an entrance grid bias of −150 V. Experimental data points are denoted by circles (○), and the curve fit by the solid line. Individual resonance peaks and the continuum step are shown by dashed lines The positions of the $\pi^*_{C=C}$, $\pi^*_{C=O}$, σ^*_{C-F} and σ^*_{C-O} resonances are indicated by +, ∇, ∗, and ◊, respectively. The C 1s → σ^*_{C-C} resonance, of the unoriented fluoroalkyl segments, occurs near 296 eV.

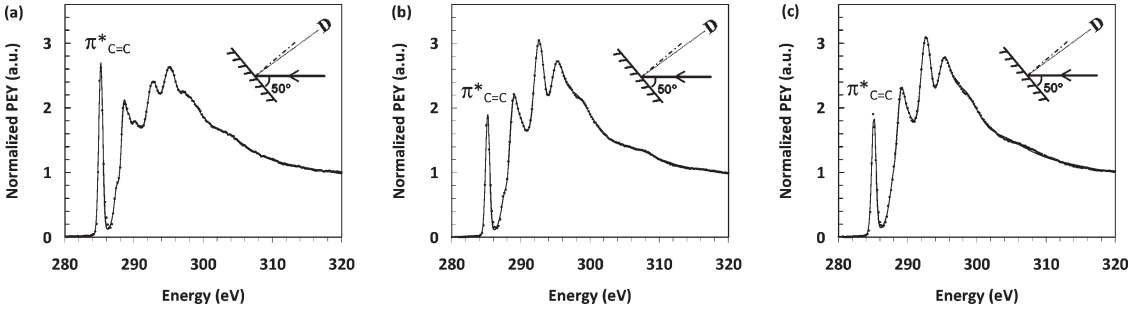

Figure 5. C 1s NEXAFS spectra of surfaces of copolymers (a) **C**, (b) **S**, and (c) **R**, obtained at an X-ray incidence angle of 50°, and an entrance grid bias of −150 V.

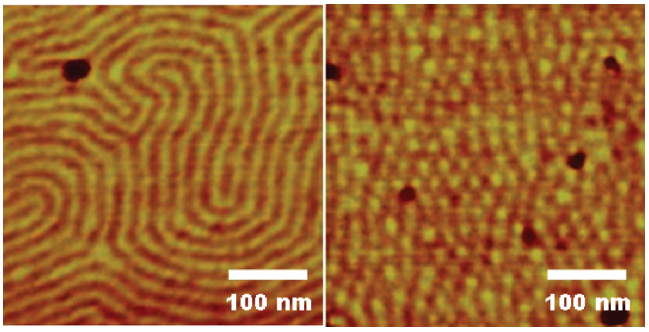

Figure 6. Tapping mode AFM phase images of "dry" films of block copolymers **C** (left) and **S** (right), on silicon surfaces.

polystyrene block, as expected.[48] However, an earlier study by Thomas and O'Malley indicated that, for both lamellar and cylinder-forming PS-*b*-PEO films, although the surfaces of the copolymer films were significantly richer in PS than in the bulk, the higher surface energy PEO was not completely covered by the lower surface energy PS block.[49] Using angle-resolved XPS experiments, they argued that the PEO domains were exposed at the air−polymer interface. Neto et al. have explained this discrepancy based on the fact that the PS-*b*-PEO films investigated by Thomas and O'Malley were not annealed, and therefore not at equilibrium, and that the thermodynamically preferred parallel arrangement was lost in the relatively thick films used in the older study.

Other researchers have reported the formation of nanopatterns of block copolymer microdomains at surfaces. Surface nanopatterns in symmetric polystyrene-*block*-poly(L-lactide) diblock copolymers have been observed using electron microscopy and AFM,[50,51] the formation of which has been attributed to the similarity in surface energy values of polystyrene and poly(L-lactide). By examining OsO_4 stained ultrathin sections of as-cast polystyrene-*block*-poly(2-hydroxyethyl methacrylate) using transmission electron microscopy, Senshu et al. found that microdomains of polystyrene and poly(2-hydroxyethyl methacrylate) were mixed at the top surface of the films.[52] The incomplete enrichment of the lower surface-energy PS at the surface was also verified using XPS. Contact angle measurements showed that the surfaces of the film became hydrophilic after soaking in water because of surface reconstruction, but the change in the surface morphology was not reversible. For symmetric polystyrene-*block*-poly[oligo(ethylene glycol) methacrylate] block copolymers, Ishizone et al. found that the nature of the terminal moiety on the oligo(ethylene glycol) (OEG) side chain, OH or OCH_3, played an important role in determining the surface structure of the block copolymer films.[53] Angle-resolved XPS and contact angle measurements indicated that whereas surfaces of block copolymers containing hydroxy-terminated OEG were completely covered by polystyrene, the poly[oligo(ethylene glycol) methacrylate] block was present at the surface of block copolymers with methoxy-terminated side chains.

In the present study, the higher C 1s $\rightarrow \pi^*_{C=C}$ peak intensity for "dry" block copolymer **C** compared to homopolymer **H**, at all X-ray incidence angles, is a clear evidence for the fact that the higher surface energy PS block was either exposed at the air−polymer interface or present within the NEXAFS probe depth of about 6 nm. Whether the presence of the higher surface energy PS block at the surface is of thermodynamic origin or of kinetic origin (that is, dependent on polarity of the solvent used for spin coating, solvent evaporation rate, annealing, or film thickness) is presently unknown. All the films used in the present study were annealed *in vacuo* at 120 °C for 12 h. Thermal annealing is expected to relax kinetically trapped morphologies, similar to those observed in other cylinder forming block copolymers, such as the poly(α-methylstyrene)-*block*-poly(4-hydroxystyrene) thin films investigated by Bosworth et al.[54] Moreover, the copolymer films used in this study were relatively thick. While a disordered microstructure, such as a mixture of cylinders oriented parallel and perpendicular to the substrate, can form in thicker films,[48] tapping mode AFM and GISAXS studies showed a well-aligned hexagonal lattice of parallel PS cylinders.[15] Regardless of whether the PS block was directly present at the air−polymer interface (as would be possible when the surface PS microdomains were laterally truncated cylinders that were not covered by the PEGylated/fluorinated block) or was buried by a very thin layer of the lower surface energy fluorinated block, our NEXAFS depth profiling analysis showed clear evidence of a lower concentration of phenyl rings at the surface, than in the bulk, for all the polymers investigated.

The volume fraction of the PEGylated/fluorinated blocks in copolymers **C** and **S** are large, but their lengths are fairly short (about 34 carbon atoms along the block length for copolymer **C**, and 40 carbon atoms for copolymer **S**). The largest possible end-to-end distances for the PEGylated/fluorinated blocks in copolymers **C** and **S** are, therefore, about 4.2 and 4.9 nm, respectively (calculated using $nl \sin(\tau/2)$, where n is the number of bonds, l is the bond length, and τ is the tetrahedral bond angle). The average side chain, in the all-*trans* (zigzag) conformation, has an end-to-end distance of about 3.2 nm. Although the actual conformations of the PEGylated/fluorinated block in the copolymer films and the fluoroalkyl−PEG side chains will have lower mean end-to-end distances than those calculated above, the calculations indicate that the side chains are not significantly smaller in length than the block length itself.[55] From this analysis, it is not unexpected that the styrene units from the PS block are present in the surface region, within the NEXAFS probe-depth, to increase the $\pi^*_{C=C}$ intenstiy, and close enough to the surface to influence surface wettability (cf. section 4.3). NEXAFS depth profiling indicates that more styrene units of the PS block were present at the surface of the block copolymer **C** with cylindrical microdomains than block copolymer **S** with spherical microdomains.

The near-surface compositional depth profiles of the block copolymers **C** and **S**, and the random copolymer, **R**, were determined using eq 9, and the experimental I_a versus θ values (please see Supporting Information for details). Both "dry" and "wet" films were characterized. The concentration profiles are shown in Figure 7.

The phenyl ring orientational order parameter, S, was found to be close to 0, indicating that the phenyl rings were only weakly oriented. Table 2 gives the average number-fraction, f_{avg}, of the phenyl ring carbon atoms (C=C carbon atoms) in the surface layer between $z/\lambda = 0$ and $z/\lambda = 2$, calculated for the concentration profiles shown in Figure 7. The values of f_{avg} for the "dry" surfaces are all greater than 6/29 (≈ 0.21), which is the average number-fraction of phenyl ring carbon atoms in homopolymer **H** based on the chemical structure of the homopolymer (cf. Figure 1). The f_{avg} values are greater than 0.21 for the dry copolymer surfaces because of the presence of phenyl rings from the styrene comonomer (in addition to the phenyl rings of the PEGylated/fluorinated monomer).[57,58]

The phenyl ring concentration was the highest for block copolymer **C** that had cylindrical PS microdomains ($f_{avg} \sim 0.37$). Block copolymer **C** had higher mole fraction of styrene units than copolymer **S** or **R** (cf. Table 1). Block copolymer **C**

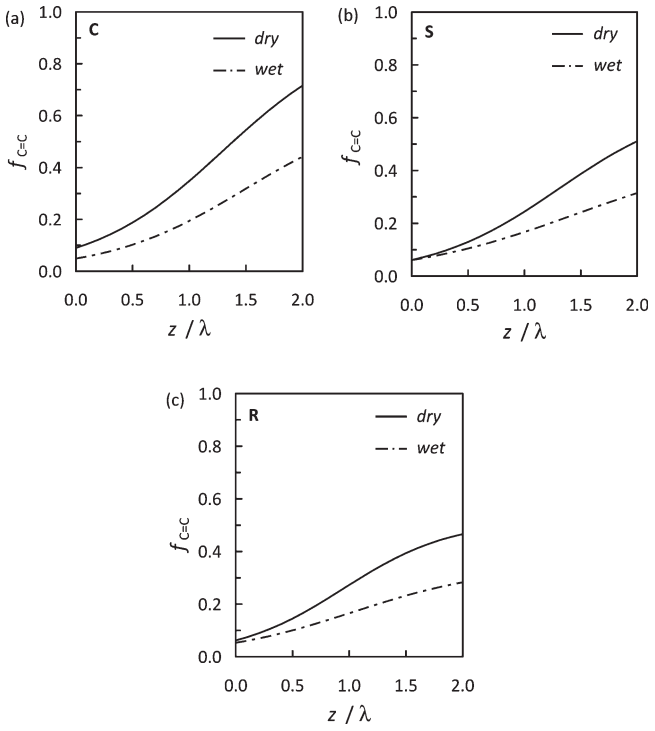

Figure 7. (a–c) Concentration depth profiles of phenyl ring carbon atoms in "dry" and "wet" thin films of copolymers **C** (a), **S** (b), and **R** (c). The electron escape depth, λ, is about 2 nm.[56]

Table 2. Phenyl Ring Peak Intensity and Average Number Fraction of Phenyl Ring Carbon Atoms at the Surface

surface	$\pi^*_{C=C}$ intensity[a]	f_{avg}[b]
dry **C**	2.66	0.37
wet **C**	1.58	0.22
dry **S**	1.86	0.26
wet **S**	1.29	0.17
dry **R**	1.84	0.27
wet **R**	1.18	0.17

[a] Postedge normalized intensity of the C 1s → $\pi^*_{C=C}$ peak at 285.2 eV and X-ray incidence angle, θ, of 50°. [b] Average of $f_{C=C}$ over the range $z/\lambda = 0$ to $z/\lambda = 2$.

also had a PEGylated/fluorinated block of a lower molecular weight. Hence, more styrene units of the PS block are expected to be present in the near-surface layer of the "dry" film of block copolymer **C** compared to the "dry" film of block copolymer **S**. The average numbers of phenyl ring carbon atoms, f_{avg}, were accordingly lower for copolymers **S** and **R** (about 0.26 and 0.27, respectively). It may be expected that copolymer **R**, with a random microstructure, would have a higher surface concentration of styrene units than the block copolymers, but the NEXAFS spectra indicate that surfaces of copolymer **R** predominantly contained the PEGylated/fluorinated styrene monomer. This can be explained by the fact that most of the film (ca. 91 vol % of the film) was composed of the PEGylated/fluorinated monomer (cf. Table 1).

In contrast to the surfaces of "dry" copolymer films, the average number-fractions of phenyl ring carbon atoms, f_{avg}, in the surface layer of all the "wet" films were close to 0.21, indicating that the copolymer surfaces, which had been soaked in water prior to NEXAFS measurements, mostly contained the PEGylated/fluorinated monomer. Upon water immersion, the concentration of the C=C carbon atoms in the surface region will increase because of migration of the PEG-grafted phenyl rings toward the surface but will

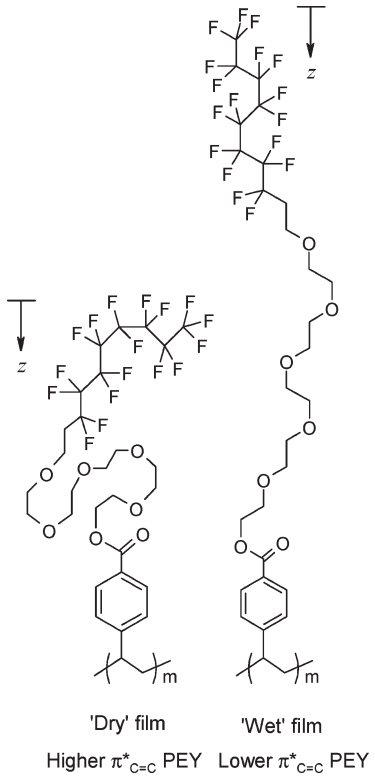

Figure 8. Schematic of side chain conformation in "dry" and "wet" films of the PEGylated/fluorinated copolymers.

decrease due to displacement of the phenyl rings of the styrene comonomer (without grafted side chains) away from the surface. Clearly, the migration of the PS block (or styrene units in the random copolymer) away from the surface causes a greater decrease in the $\pi^*_{C=C}$ signal than the increase due to the migration of PEG-tethered phenyl rings toward the surface.

The average number of phenyl ring carbon atoms at surfaces of the "wet" films of copolymers **S** and **R** is lower than the stoichiometric value of 0.21 because of the displacement of the phenyl rings away from the polymer surface by the PEGylated side chains that adopted an extended conformation when contacted with water (cf. Figure 8).

In the following sections, a more detailed discussion of the surface composition of the copolymer thin films and the surface reconstruction after water immersion is reported.

Block Copolymer with Cylindrical Nanostructures. Figure 9 compares the NEXAFS spectra of "dry" and "wet" films of block copolymer **C**, obtained at incidence angles of 50° and 130°. The complete set of NEXAFS spectra, including those obtained at other X-ray incidence angles, are available as Supporting Information.

Figure 10 shows the experimental $\pi^*_{C=C}$ resonance intensities at different X-ray incidence angles, for the "dry" and the "wet" films, and the best fit I_a vs θ curves that correspond to the composition profiles shown in Figure 7a. A large decrease in the $\pi^*_{C=C}$ resonance intensity is observed for the water-immersed sample, at all angles of X-ray incidence. There is a corresponding increase in the intensities of the $\pi^*_{C=O}$, σ^*_{C-F}, and σ^*_{C-O} resonances in the "wet" samples (cf. Figure 9). The decrease in the $\pi^*_{C=C}$ resonance intensity and the increase in the $\pi^*_{C=O}$, σ^*_{C-F}, and σ^*_{C-O} peak heights is attributed to the migration of the phenyl rings away from the surface and the PEGylated fluoroalkyl side chains toward the surface.

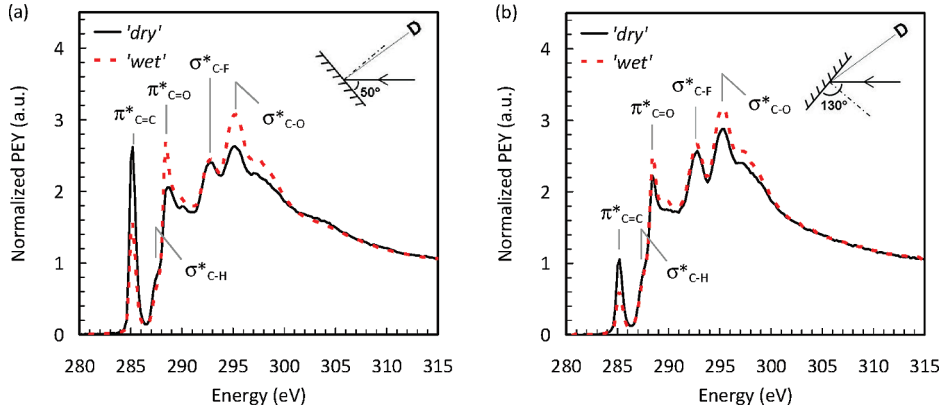

Figure 9. C 1s NEXAFS spectra of "dry" and "wet" thin films of block copolymer **C**, acquired at X-ray incidence angles of (a) 50° and (b) 130° and an entrance grid bias of −150 V.

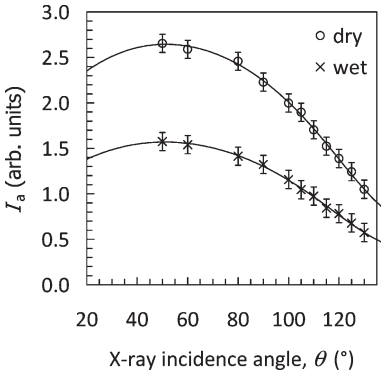

Figure 10. Intensity of the C 1s → $\pi^*_{C=C}$ resonance as a function of the X-ray incidence angle for "dry" and "wet" thin films of block copolymer **C**; EGB = −150 V. The solid lines are best fit curves for the model discussed in Supporting Information.

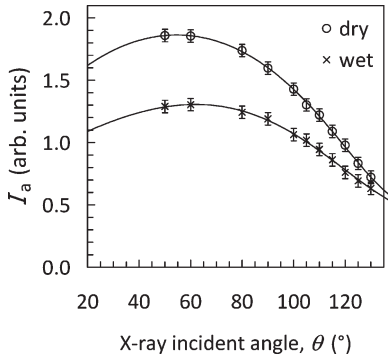

Figure 11. Intensity of the C 1s → $\pi^*_{C=C}$ resonance as a function of the X-ray incidence angle for "dry" and "wet" thin films of block copolymer **S**; EGB = −150 V.

Block Copolymer Thin Films with Spherical Nanostructures. Figure 11 shows a comparison of the $\pi^*_{C=C}$ peak intensities at different X-ray incidence angles for the "dry" and "wet" surfaces of polymer **S**. The solid lines are best fit curves, determined as described in Supporting Information.

In the case of block copolymer **S**, the spherical microdomains of the PS block were completely covered by the PEGylated/fluorinated block, resulting in lower $\pi^*_{C=C}$ resonance intensities and f_{avg} values than for block copolymer **C**. When the film contacted water, surface reconstruction occurred at the level of individual PEGylated/fluorinated monomer, as shown in Figure 8. There was an overall decrease in the concentration of phenyl rings in the vicinity of the surface.

Random Copolymer. The C 1s NEXAFS spectra of the "dry" and wet thin films of the random copolymer, **R**, are shown in Figure 12. The normalized $\pi^*_{C=C}$, for all the X-ray incidence angles used, are shown in Figure 13. As in the case of polymers **H**, **S**, and **C**, the $\pi^*_{C=C}$ intensities are lower when the X-ray incidence was at 130° than at 50°. Although the average number-fraction of phenyl ring carbon atoms is significantly lower in random copolymer **R** ($f_b \sim 0.275$) than block copolymer **S** ($f_b \sim 0.432$), their surface composition is fairly similar (f_{avg} is about 0.26 for **S** and about 0.27 for **R**). Thus, block architecture of the copolymer can produce surface concentration profiles that are similar to a random architecture, but at a significantly lower number fraction of the PEGylated/fluorinated surface-active monomer, a result that is of relevance in designing practical coatings for large surfaces such as ship hulls.

4.3. Surface Wettability. Advancing and receding water contact angles were measured on the "dry" polymer films. These thermally annealed films were sufficiently smooth, with AFM root-mean-square surface roughness values equal to 1.7 nm for dry **C** and 0.98 nm for dry **S**. Thus, the difference between the advancing contact angle, θ_a, and the receding contact angle, θ_r, characterizes rapid surface reconstruction, and in the case of the copolymers, any surface chemical heterogeneity, rather than surface roughness. The advancing and receding angles on homopolymer **H** were 120 ± 2° and 22 ± 4°, respectively, indicating rapid, reversible surface reconstruction. The θ_a and θ_r values at a particular spot on the surface did not change noticeably with repeated expansion and contraction of the water droplet at that spot, suggesting that the surface reconstruction was reversible over the time scale of the dynamic contact angle experiment. For block copolymer **C**, θ_a was 101 ± 1° and θ_r was 50 ± 1°. A significant influence of the PS block on the water contact angle values is evident, as expected from the NEXAFS spectra of the dry film (which show a pronounced $\pi^*_{C=C}$ peak from phenyl rings and a less distinct σ^*_{C-F} peak from the fluoroalkyl segments of the side chains). Polystyrene homopolymer has $\theta_a = 94 \pm 4°$ and $\theta_r = 81 \pm 3°$. The surface PS component of block copolymer **C** lowers the advancing contact angle and raises the receding contact angle relative to homopolymer **H**. The contact angles on block copolymer **S**, on the other hand, were closer to those on homopolymer **H** (θ_a and θ_r of 108 ± 1° and 44 ± 2°, respectively, for "dry" **S**). The random copolymer **R** gave an advancing contact angle value near that on homopolymer **H** and a receding contact angle somewhat closer to the value on polystyrene ($\theta_a = 114 \pm 2°$ and $\theta_r = 60 \pm 2°$ for "dry" **R**).

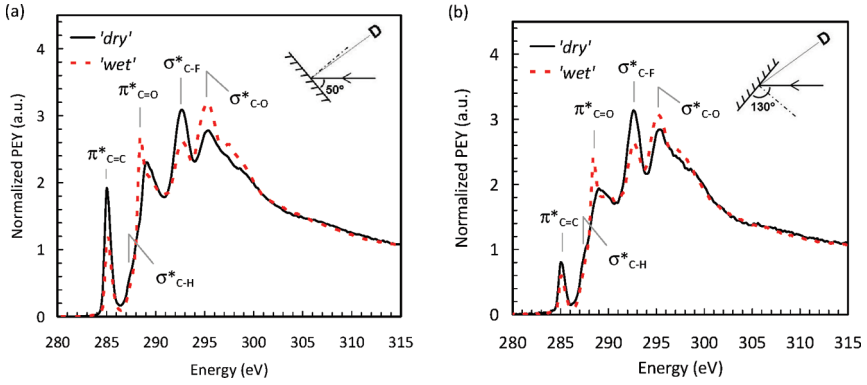

Figure 12. C 1s NEXAFS spectra of "dry" and "wet" thin films of random copolymer **R**, acquired at X-ray incidence angles of (a) 50° and (b) 130° and an entrance grid bias of −150 V.

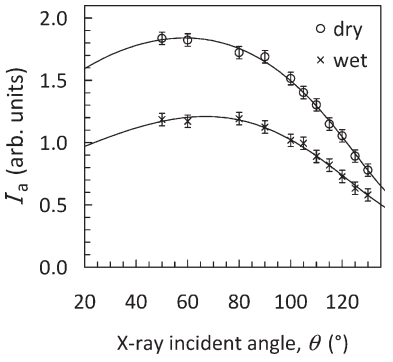

Figure 13. Intensity of the C 1s → $\pi^*_{C=C}$ resonance as a function of the X-ray incidence angle for "dry" and "wet" thin films of random copolymer **R**; EGB = −150 V.

In summary, the dynamic water contact angles are significantly influenced by the microstructure of the copolymer in the film, and by the surface composition.[59−62]

5. Conclusions

We have used NEXAFS spectroscopy to study molecular organization at surfaces of polymers containing PEGylated fluoroalkyl side chains. The depth profiling technique described in this paper was used to obtain the composition profile in the top few nanometers of the polymer thin films and determine the average surface concentration of phenyl ring carbon atoms. A homopolymer of the PEGylated/fluorinated monomer and its copolymers with styrene were studied. Both random copolymer and block copolymer thin films were probed. In all the polymer films investigated, the low surface energy fluoroalkyl segments of the side chains showed segregation to the polymer−air interface, dragging along the relatively high surface-energy PEG groups. In the case of diblock copolymer thin films, it is generally expected that the block with lower surface energy will be present at the surface, completely covering the higher surface energy block. However, NEXAFS spectra of the cylinder-forming block copolymer film clearly showed the presence of the higher surface energy polystyrene block in the near surface region ($z \lesssim 4$ nm). The block copolymer with spherical microdomains, on the other hand, presented mainly the lower energy fluorinated block at the air−polymer interface. Evidently, spherical microdomains can be more effectively covered by a lower surface energy brush layer than wormlike cylindrical microdomains. Moreover, the sphere-forming block copolymer showed similar surface composition and concentration profile as a random copolymer, at a significantly lower content of the PEGylated/fluorinated monomer.

All surfaces showed surface reconstruction after immersion in water. The composition depth profiles showed significant differences before and after water treatment. The polymer films showed migration of phenyl rings away from the surface after water immersion. In the case of block copolymers, the decrease in the intensity of the $\pi^*_{C=C}$ resonance is mainly due to migration of the PS domains away from the polymer interface, which explains the relatively slow kinetics of this surface reconstruction process. Surface wettability measurements have shown an under-water reconstruction that occurs over a period of several hours.[7,15] A faster surface reconstruction, which can be inferred from dynamic water contact angle measurements, occurs by flipping of the side chains such that the perfluoroalkyl segments rearrange to accommodate the PEG segments that are preferred at the polymer−water interface.

In conclusion, contrary to expectations that the surfaces of block copolymer coatings will be completely covered by a lamellar layer of the block with lower surface energy, the present study shows that it may be possible to at least partially expose the higher surface energy block at the polymer interface. Such block copolymer coatings may find use in biomedical applications where nanoscale chemical heterogeneity is sought, for example, in preventing protein adsorption on surfaces.

Acknowledgment. Use of the National Synchrotron Light Source, Brookhaven National Laboratory, was supported by the U.S. Department of Energy Office of Science, Office of Basic Energy Sciences. S.K. would like to thank Dr. Jonathan Shu for help with XPS data acquisition using facilities at the Cornell Center for Materials Research, a Materials Research Science and Engineering Center funded by the National Science Foundation. S.K. gratefully acknowledges partial support from the Army Research Office grant W911NF-05-1-0339. The Office of Naval Research grant N00014-02-1-0170 to C.K.O. and E.J.K., and the Department of Defense's Strategic Environmental Research and Development Program (SERDP) grant WP-1454 to C.K.O. are also acknowledged. E.M. and G.G. thank the EU for financial support through Framework 6 Integrated Project AMBIO (Advanced Nanostructured Surfaces for the Control of Biofouling). K.E.S. and E.J.K. acknowledge partial support from an NSF Graduate Fellowship and the NSF Polymers Program (DMR-0704539).

Supporting Information Available: Text discussing and figures showing the C 1s XPS spectrum of the PEGylated/fluorinated homopolymer, angle resolved XPS spectra of block copolymer surfaces, postedge normalized NEXAFS spectra of "dry" and "wet" copolymer thin films acquired at X-ray incidence angles ranging from 50 to 130°, NEXAFS spectra to show absence of surface reconstruction in wet surfaces during NEXAFS spectra acquisition, the mathematical model assumed for concentration profile of phenyl ring carbon atoms, and details (including a table) on determining model parameters

from experimental data. This material is available free of charge via the Internet at http://pubs.acs.org.

References and Notes

(1) Martinelli, E.; Agostini, S.; Galli, G.; Chiellini, E.; Glisenti, A.; Pettitt, M. E.; Callow, M. E.; Callow, J. A.; Graf, K.; Bartels, F. W. *Langmuir* **2008**, *24*, 13138–13147.

(2) Grozea, C. M.; Gunari, N.; Finlay, J. A.; Grozea, D.; Callow, M. E.; Callow, J. A.; Lu, Z.-H.; Walker, G. C. *Biomacromolecules* **2009**, *10*, 1004–1012.

(3) Gudipati, C. S.; Greenlief, C. M.; Johnson, J. A.; Prayongpan, P.; Wooley, K. L. *J. Polym. Sci., Part A: Polym. Chem.* **2004**, *42*, 6193–6208.

(4) Gudipati, C. S.; Finlay, J. A.; Callow, J. A.; Callow, M. E.; Wooley, K. L. *Langmuir* **2005**, *21*, 3044–3053.

(5) Finlay, J. A.; Krishnan, S.; Callow, M. E.; Callow, J. A.; Dong, R.; Asgill, N.; Wong, K.; Kramer, E. J.; Ober, C. K. *Langmuir* **2008**, *24*, 503–510.

(6) Krishnan, S.; Wang, N.; Ober, C. K.; Finlay, J. A.; Callow, M. E.; Callow, J. A.; Hexemer, A.; Sohn, K. E.; Kramer, E. J.; Fischer, D. A. *Biomacromolecules* **2006**, *7*, 1449–1462.

(7) Krishnan, S.; Ayothi, R.; Hexemer, A.; Finlay, J. A.; Sohn, K. E.; Perry, R.; Ober, C. K.; Kramer, E. J.; Callow, M. E.; Callow, J. A.; Fischer, D. A. *Langmuir* **2006**, *22*, 5075–5086.

(8) Weinman, C. J.; Finlay, J. A.; Park, D.; Paik, M. Y.; Krishnan, S.; Sundaram, H. S.; Dimitriou, M.; Sohn, K. E.; Callow, M. E.; Callow, J. A.; Willis, C. L.; Kramer, E. J.; Ober, C. K. *Langmuir* **2009**, *25*, 12266–12274.

(9) Vaidya, A.; Chaudhury, M. K. *J. Colloid Interface Sci.* **2002**, *249*, 235–245.

(10) Makal, U.; Uslu, N.; Wynne, K. J. *Langmuir* **2007**, *23*, 209–216.

(11) Jannasch, P. *Macromolecules* **1998**, *31*, 1341–1347.

(12) Russell, T. P. *Science* **2002**, *297*, 964–967.

(13) Luzinov, I.; Minko, S.; Tsukruk, V. V. *Prog. Polym. Sci.* **2004**, *29*, 635–698.

(14) Koberstein, J. T. *J. Polym. Sci., Part B: Polym. Phys.* **2004**, *42*, 2942–2956.

(15) Martinelli, E.; Menghetti, S.; Galli, G.; Glisenti, A.; Krishnan, S.; Paik, M. Y.; Ober, C. K.; Smilgies, D.-M.; Fischer, D. A. *J. Polym. Sci., Part A: Polym. Chem.* **2008**, *47*, 267–284.

(16) Theato, P.; Brehmer, M.; Conrad, L.; Frank, C. W.; Funk, L.; Yoon, D. Y.; Lüning, J. *Macromolecules* **2006**, *39*, 2592–2595.

(17) Weinman, C. J.; Krishnan, S.; Park, D.; Paik, M. Y.; Wong, K.; Fischer, D. A.; Handlin, D. L., Jr.; Kowalke, G. L.; Wendt, D. E.; Sohn, K. E.; Kramer, E. J.; Ober, C. K. *Polym. Mater Sci. Eng. Prepr.* **2007**, *96*, 597–598.

(18) Liu, X.; Mao, Y.; Mathias, E. V.; Ma, C.; Franco, O.; Ba, Y.; Kornfield, J. A.; Wang, T.; Xue, L.; Zhou, B.-S.; Yen, Y. *J. Sol-Gel Sci. Technol.* **2008**, *45*, 269–278.

(19) Howarter, J. A.; Youngblood, J. P. *J. Colloid Interface Sci.* **2009**, *329*, 127–132.

(20) Krishnan, S.; Kwark, Y.-J.; Ober, C. K. *Chem. Rec.* **2004**, *4*, 315–330.

(21) Krausch, G. *Mater. Sci. Eng., R.* **1995**, *R14*, 1–94.

(22) Bucknall, D. G. *Prog. Mater. Sci.* **2004**, *49*, 713–786.

(23) Kramer, E. J. *Physica B* **1991**, *173*, 189–198.

(24) Kerle, T.; Scheffold, F.; Losch, A.; Steiner, U.; Schatz, G.; Klein, J. *Acta Polym.* **1997**, *48*, 548–552.

(25) Wang, C.; Araki, T.; Watts, B.; Harton, S.; Koga, T.; Basu, S.; Ade, H. *J. Vac. Sci. Technol. A* **2007**, *25*, 575–586.

(26) Gagnon, D. R.; McCarthy, T. J. *J. Appl. Polym. Sci.* **1984**, *29*, 4335–4340.

(27) Cross, E. M.; McCarthy, T. J. *Macromolecules* **1990**, *23*, 3916–3922.

(28) Tyler, B. J.; Castner, D. G.; Ratner, B. D. *Surf. Interface Anal.* **1989**, *14*, 443–450.

(29) Senshu, K.; Yamashita, S.; Mori, H.; Ito, M.; Hirao, A.; Nakahama, S. *Langmuir* **1999**, *15*, 1754–1762.

(30) Beamson, G.; Alexander, M. R. *Surf. Interface Anal.* **2004**, *36*, 323–333.

(31) Dwyer, V. M. *Surf. Interface Anal.* **1994**, *21*, 637–642.

(32) For example, see: Teruaki, H.; Wang, J.; Xiang, M.; Li, X.; Mitsuru, U.; Ober, C. K.; Genzer, J.; Sivaniah, E.; Kramer, E. J.; Fischer, D. A. *Macromolecules* **2000**, *33*, 8012–8019.

(33) Zentel and coworkers have further investigated surface construction in a library of block copolymers with different functional side chains using contact angle measurements and AFM; cf.: Funk, L.; Brehmer, M.; Zentel, R.; Kang, H.; Char, K. *Macromol. Chem. Phys.* **2008**, *209*, 52–63.

(34) Molar volume of the PEGylated/fluorinated homopolymer is $(153.5 + 45.7x + 30.7y)$ cm^3/mol where x and y are the average numbers of ethylene glycol and perfluoroethylene groups, respectively, in each monomer: Bicerano, J. *Prediction of Polymer Properties*, 2nd ed.; Marcel Dekker: New York, 1996.

(35) Specular reflection of the incident X-ray beam, by the sample onto the detector, occurs at an X-ray incidence angle of 72°. Although specular reflection is expected to affect only fluorescence yield measurements, we found that the electron yield was also affected. Hence, $\theta = 70°$ was not used in our analysis.

(36) Stöhr, J. Analysis of K-shell excitation spectra by curve fitting. In *NEXAFS Spectroscopy*; Springer Series in Surface Science 25; Springer: New York, 1992; p 211.

(37) Rosenberg, R. A.; Love, P. J.; Rehn, V. *Phys. Rev. B: Condens. Matter Mater. Phys.* **1986**, *33*, 4034–4037.

(38) Krishnan, S.; Ober, C. K.; Hexemer, A.; Kramer, E. J.; Fischer, D. A. *Polym. Mat. Sci. Eng. Prepr.* **2006**, *94*, 672–673.

(39) Lenhart, J. L.; Fischer, D. A.; Sambasivan, S.; Lin, E. K.; Jones, R. L.; Soles, C. L.; Wu, W.-L.; Goldfarb, D. L.; Angelopoulos, M. *Langmuir* **2005**, *21*, 4007–4015.

(40) Klein, R. J.; Fischer, D. A.; Lenhart, J. L. *Langmuir* **2008**, *24*, 8187–8197.

(41) Stöhr, J. The anglular dependence of resonance intensities. In *NEXAFS Spectroscopy*; Springer Series in Surface Science 25; Springer: New York, 1992; p 276.

(42) For thin films of perfluorinated polyether on graphite, Sohn et al. demonstrated that the depth variation of carbon atom density must be considered for accurate compositional depth profiling using NEXAFS (ref 43). However, the simplifying assumption of depth-invariant carbon atom density is believed to be satisfactory for comparison of surface compositions of the polymers used in the present study (cf. Supporting Information).

(43) Sohn, K. E.; Dimitriou, M. D.; Genzer, J.; Fischer, D. A.; Hawker, C. J.; Kramer, E. J. *Langmuir* **2009**, *25*, 6341–6348.

(44) The C 1s $\rightarrow \pi^*_{C=C}$ peak near 285.2 eV has contributions from carbon atoms of the phenyl rings in the PEGylated/fluorinated monomer, and in the copolymer, also from the phenyl ring carbon atoms of the styrene monomer.

(45) In using eq 9 for the copolymer surfaces, we have assumed that the phenyl ring carbon atoms in polystyrene and the phenyl ring carbon atoms in the PEGylated/fluorinated monomer have the same X-ray absorption cross sections. The effect of the side group on the C 1s $\rightarrow \pi^*_\Phi$ resonance intensity of the PEGylated/fluorinated monomer can only be through the penultimate carbon atom (of the ester linkage), and was found to be negligible. Evidently, the phenyl rings in the copolymers of the present study are different from the C=C carbon atoms in heterocyclic rings such as those in poly(4-vinylpyridine) or poly(*N*-hexyl-4-vinylpyridinium bromide). For the pyridinium polymers, we had previously reported that the electronegative nitrogen atoms present in the aromatic ring not only cause a split in the C 1s $\rightarrow \pi^*_\Phi$ resonance peak (corresponding to differences in electron densities of the *ortho* and *meta* carbon atoms) but also cause a lower C 1s $\rightarrow \pi^*_\Phi$ peak intensity compared to that of polystyrene (cf. ref 46). However, in the present study, the widths of the C 1s $\rightarrow \pi^*_\Phi$ resonance peaks of the copolymers were similar to those of the styrene and PEGylated/fluorinated styrene homopolymers. The X-ray absorption cross-section of the phenyl ring carbon atoms of the PEGylated/fluorinated styrene copolymers, determined using the experimental I_a vs θ data, were found to be same as that of polystyrene phenyl ring carbon atoms.

(46) Krishnan, S.; Ward, R. J.; Hexemer, A.; Sohn, K. E.; Lee, K. L.; Angert, E. R.; Fischer, D. A.; Kramer, E. J.; Ober, C. K. *Langmuir* **2006**, *22*, 11255–11266.

(47) Khanna, V.; Cochran, E. W.; Hexemer, A.; Stein, G. E.; Fredrickson, G. H.; Kramer, E. J.; Li, X.; Wang, J.; Hahn, S. F. *Macromolecules* **2006**, *39*, 9346–9356.

(48) Neto, C.; James, M.; Telford, A. M. *Macromolecules* **2009**, *42*, 4801–4808.

(49) Thomas, H. R.; O'Malley, J. J. *Macromolecules* **1979**, *12*, 323–329.

(50) Chen, D.; Gong, Y.; Huang, H.; He, T. *Macromolecules* **2007**, *40*, 6631–6637.

(51) Olayo-Valles, R.; Guo, S.; Lund, M. S.; Leighton, C.; Hillmyer, M. A. *Macromolecules* **2005**, *38*, 10101–10108.

(52) Senshu, K.; Yamashita, S.; Ito, M.; Hirao, A.; Nakahama, S. *Langmuir* **1995**, *11*, 2293–2300.

(53) Ishizone, T.; Han, S.; Hagiwara, M.; Yokoyama, H. *Macromolecules* **2006**, *39*, 962–970.

(54) Bosworth, J. K.; Paik, M. Y.; Ruiz, R.; Schwartz, E. L.; Huang, J. Q.; Ko, A. W.; Smilgies, D.-M.; Black, C. T.; Ober, C. K. *ACS Nano* **2008**, *2*, 1396–1402.
(55) The PS block is also comparable in size to the PEGylated/fluorinated block. The average number of carbon atoms along the backbone of the PS block is about 102. The root mean-square end-to-end distance, and the radius of gyration, of a PS homopolymer of this length is 4.6 and 1.9 nm, respectively.
(56) Inelastic collision of an Auger electron results in a cascade of electrons produced by secondary electron emission processes. Most of these electrons have kinetic energies (KE) lower than the entrance grid bias of the detector (equal to −150 V), and are filtered off by the entrance grid. A small fraction of the inelastically scattered primary Auger electrons and the secondary electrons of the cascade, which have KE greater than 150 eV, can nevertheless get past the entrance grid and contribute to the partial electron yield. The fact that even some inelastically scattered electrons can contribute to the NEXAFS signal results in a higher probe-depth in NEXAFS depth-profiling than what can be achieved by detecting only unscattered electrons. The value electron escape depth has therefore been expected to be greater than IMFP, and a value of 1.95 nm has been reported for a perfluropolyether (Fomblin Z-03) thin film (cf. ref 43).
(57) The f_{avg} values are, however, lower than $f_{C=C}$ in the bulk ($= f_b$). The values of f_b for the copolymers **C**, **S**, and **R**, calculated using the compositions shown in Table 1, are 0.453, 0.432, and 0.275, respectively (cf. ref 58). $f_{avg} < f_b$ for the "dry" copolymer surfaces because of surface segregation of the fluorinated side chains.
(58) Based on the chemical structure of the copolymer shown in Figure 1, the total number of carbon atoms in each copolymer molecule is equal to $8n + (11 + 2x + 2y)m$, or $8n + 29m$ since $x = 5$ and $y = 4$. The total number of phenyl ring carbon atoms is equal to $6n + 6m$. Therefore, the number fraction of phenyl ring carbon atoms in the bulk, f_b, which is expected to be equal to the stoichiometric number fraction of phenyl ring carbon atoms in the copolymer, is given by $6(n + m)/(8n + 29m)$.
(59) The Cassie−Baxter equation has been widely applied to chemically heterogeneous surfaces composed of two polymers, each characterized by its own contact angle θ_1 and θ_2. For example, see references 60−62.The equation predicts that the contact angle, θ^*, on the heterogeneous surface will be given by $\cos\theta^* = f_1 \cos\theta_1 + f_2 \cos\theta_2$, where f_1 and f_2 are the fractions of the two polymers at the surface ($f_1 + f_2 = 1$). The surface compositions determined using NEXAFS spectroscopy indicate that this equation is not applicable to the copolymer surfaces of the present study, at least in the form stated above, because of surface reconstruction during the measurement of the contact angles.
(60) Yuan, Y.; Shoichet, M. S. *Macromolecules* **2000**, *33*, 4926–4931.
(61) Whyman, G.; Bormashenko, E.; Stein, T. *Chem. Phys. Lett.* **2008**, *450*, 355–359.
(62) Julthongpiput, D.; Lin, Y.-H.; Teng, J.; Zubarev, E. R.; Tsukruk, V. V. *Langmuir* **2003**, *19*, 7832–7836.